Measuring the Total Photon Economy of Molecular Species through Fluorescent Optical Cycling - Supplemental Information

Anthony V. Sica,[§] Ash Sueh Hua,[§] Belle Coffey, Kierstyn P. Anderson, Lia A. Coffey, Benjamin T. Nguyen, Alexander M. Spokoyny, and Justin R. Caram[*]

Department of Chemistry and Biochemistry, University of California, Los Angeles, 607 Charles E. Young Drive, Los Angeles, California 90095-1569, USA

Table of Contents

I. Materials

All solvents including acetic acid, acetone, acetonitrile, dichloromethane, diiodomethane, and ethanol were purchased from Fischer Scientific. 2-(2-thienyl)pyridine (thpy) was purchased from TCI chemicals. Potassium tetrachloroplatinate(II), 1,1-bis(diphenylphosphino)methane (dppm), lithium perchlorate, and deuterated dichloromethane were purchased from Sigma Aldrich. Rose Bengal was purchased from Kodak.

II. Absorption and Emission Measurements

UV-vis measurements were taken on an Agilent Cary 60 UV-Vis spectrometer. Emission measurements were taken on a Horiba Scientific PTI QuantaMaster400 Spectrometer with a Si photomultiplier tube for UV-visible region detection and a liquid nitrogen cooled InGaAs photodiode for IR region detection.

III. FOC Hardware Timing Specifications

Table S1. FOC Hardware Timing Specifications

Hardware	Timing Jitter (ps)
PDL 800D internal oscillator (80 MHz)	3-5
PDL 800D sync output	< 20
SRS DG535 delay channel	60 + (delay $\times 10^{-8}$)
SRS DG535 channel-channel jitter	50
MPD PDM	< 50

IV. Kinetic Modeling

A kinetic model is used for fitting and understanding FOC traces. A simplified three state model is used to depict the ground state (S_0), singlet excited state (S_1), and the triplet excited state (T_1) (Figure 2a). Included in this model are rates for total fluorescence, total phosphorescence, intersystem crossing (ISC), and reverse intersystem crossing (k_f, k_p, k_{ISC}, k_{rISC}, respectively). These processes are summarized below.

$$S_1 \underset{k_{rISC}}{\overset{k_{ISC}}{\rightleftharpoons}} T_1,\ S_1 \xrightarrow{k_f} S_0,\ T_1 \xrightarrow{k_p} S_0 \tag{S1}$$

Each laser pulse moves a percentage of population from the ground state to the singlet excited state, reflecting a fixed per molecule cross-section at the excitation energy. Between every pulse, the kinetics of each state are described with the following differential equations:

$$\frac{\partial[S_0]}{\partial t} = k_p[T_1] + k_f[S_1] \tag{S2}$$

$$\frac{\partial[S_1]}{\partial t} = k_{rISC}[T_1] - (k_f + k_{ISC})[S_1] \tag{S3}$$

$$\frac{\partial[T_1]}{\partial t} = -\left(k_p + k_{rISC}\right)[T_1] + k_{ISC}[S_1] \tag{S4}$$

Differentiation of (S2) and substitution of $[T_1]$ terms for $[S_1]$ terms results in a 2nd order differential equation.

$$0 = \frac{\partial^2}{\partial t^2}[S_1] + (k_{ISC} + k_{rISC} + k_f + k_p)\frac{\partial}{\partial t}[S_1] + (k_{ISC}k_p + k_{rISC}k_f + k_f k_p)[S_1] \tag{S5}$$

$$a = 1,\ b = \left(k_{ISC} + k_{rISC} + k_f + k_p\right),\ c = (k_{ISC}k_p + k_{rISC}k_f + k_f k_p)$$

The roots, $r_{(\pm)}$, of the resulting characteristic equation (S4) are as follows, where D is the determinant of the roots.

$$r_{(\pm)} = \frac{-\left(k_{ISC} + k_{rISC} + k_f + k_p\right) \pm \sqrt{D}}{2} \tag{S6}$$

$$D = \left(k_{ISC} + k_{rISC} + k_f + k_p\right)^2 - 4(k_{ISC}k_p + k_{rISC}k_f + k_f k_p) \tag{S7}$$

The general solution to the differential equation, (S7), and the first derivative of the general solution, (S8) is as follows.

$$[S_1] = C_{(+),S_1}\exp\left(r_{(+)}t\right) + C_{(-),\,S_1}exp(r_{(-)}t) \tag{S8}$$

$$\frac{\partial[S_1]}{\partial t} = C_{(+),S_1}\mathrm{r}_{(+)}\exp\left(r_{(+)}t\right) + C_{(-),\,S_1}r_{(-)}exp(r_{(-)}t) \tag{S9}$$

Using the initial values of $[S_1](t=0) = [S_1]_i$ and $[T_1](t=0) = [T_1]_i$, the constants $C_{(\pm),S_1}$ for the solution are found.

$$C_{(\pm),S_1} = \frac{1}{2\sqrt{D}}\left\{\left[\mp\left(k_{ISC} - k_{rISC} + k_f - k_p\right) + \sqrt{D}\right][S_1]_i \pm 2k_{rISC}[T_1]_i\right\} \tag{S10}$$

To solve for $[T_1]$, substitution of the solutions to $[S_1]$ and $\frac{\partial[S_1]}{\partial t}$ into (S2) yields a solution with the same general form but with different constants.

$$[T_1] = C_{(+),T_1}\exp\left(r_{(+)}t\right) + C_{(-),T_1}exp(r_{(-)}t) \tag{S11}$$

$$C_{(\pm),T_1} = \frac{1}{2\sqrt{D}}\left\{\left[\pm\left(k_{ISC} - k_{rISC} + k_f - k_p\right) + \sqrt{D}\right][T_1]_i \pm 2k_{ISC}[S_1]_i\right\} \tag{S12}$$

V. FOC Traces from Kinetic Modeling

The parameters shown below were used in generating the FOC traces in Figure 2b-e.

Table S2. Rates and other parameters used in modeling FOC traces.

		k_f (s^{-1} x 10^9)	k_p (s^{-1} x 10^6)	k_{ISC} (s^{-1} x 10^6)	k_{rISC} (s^{-1} x 10^6)	k_σ (%)	$k_{\phi Dep.}$ (%)
2b	Red	0.2	0.4	0.05	0	95	0
	Blue	0.2	0.4	20	0	95	0
2c	Red	0.2	4.0	20	0	95	0
	Blue	0.2	0.4	20	0	95	0
2d	Red	0.2	0.4	20	0	9	0
	Blue	0.2	0.4	20	0	90	0
2e	Red	0.2	0.4	20	0	95	90
	Blue	0.2	0.4	20	0	95	0

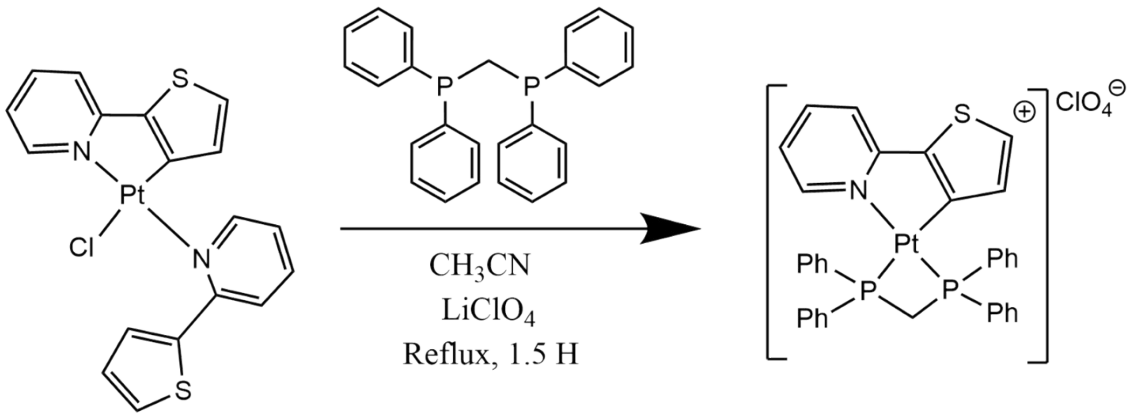

VI. Synthesis of Platinum Complex [Pt(thpy)(dppm)]ClO_4

[Pt(thpy)(μ-thpy)Cl] was synthesized according to published procedure.[1,2] The subsequent synthesis of [Pt(thpy)(dppm)]ClO_4 was adapted from published procedure.[3] [Pt(thpy)(μ-thpy)Cl] (0.49 grams, 0.90 mmol) was dissolved in 15 mL of acetonitrile. 1,1-bis(diphenylphosphino)methane (0.345 g, 0.90 mmol) was added to the stirring solution in a 1:1 molar ratio to the [Pt(thpy)(μ-thpy)Cl]. The resulting solution was heated at reflux under argon

flow for one hour. After one hour, 3.0 molar equivalents of $LiClO_4$ (0.28 g, 2.7 mmol) were added to the solution. The solution was kept under argon and at reflux for an additional 30 minutes, and then allowed to cool to room temperature. The solvent was removed via rotary evaporation. The resulting orange solid was purified via column chromatography with a 10:1 DCM:acetone solution as the eluent. After purification, the remaining solvent was removed via rotary evaporation. The isolated orange powder was vacuum dried and then characterized via ^{1}HNMR spectroscopy (400 MHz Bruker). ^{1}HNMR 400 MHz (CD_2Cl_2): δ 4.78 (t with broad ^{195}Pt satellites, $J_{H\text{-}H}$ = 10.7 Hz, 2H, CH_2), 6.43 (m, 1H), 7.05 (t, J = 6.3 Hz, 1H), 7.34 (dd, J = 4.3, 1.8 Hz, 1H), 7.51 (m, 8H, PPh_2), 7.59 (m, 5H), 7.76 (m, 8H, PPh_2), 7.92 (td, J = 7.8, 1.3 Hz, 1H), 8.24 (t with broad ^{195}Pt satellites, $J_{H\text{-}H}$ = 4.7 Hz, 1H). ^{31}P{^{1}H} NMR (CD3CN): -38.33 (d, $J_{P\text{-}P}$ = 47.5 Hz), -30.08, (d, $J_{P\text{-}P}$ = 47.4 Hz).

VII. ^{1}H NMR Spectrum of Platinum Complex [Pt(thpy)(dppm)]ClO_4

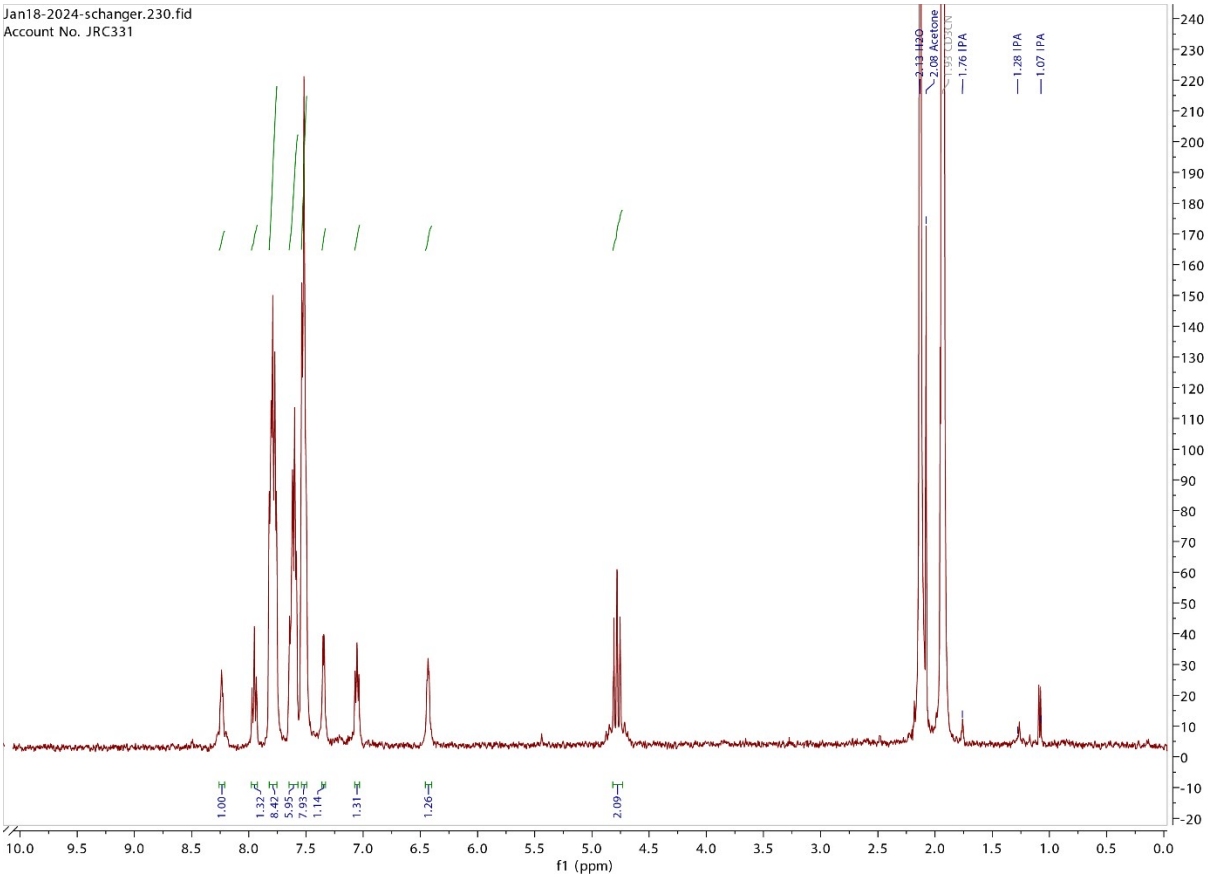

VIII. ^{31}P NMR Spectrum of Platinum Complex [Pt(thpy)(dppm)]ClO_4

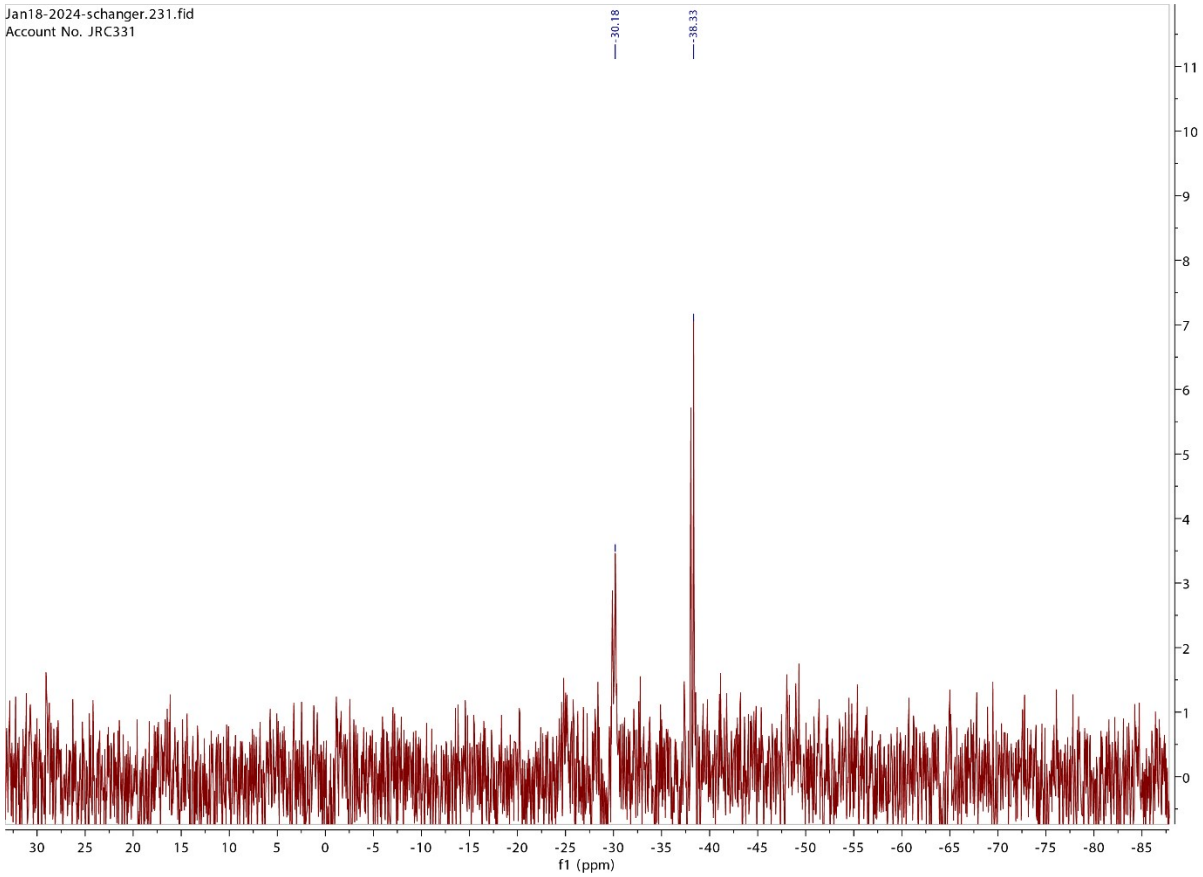

IX. [Pt(thpy)(dppm)]ClO_4 Emission Spectra EHAE Series

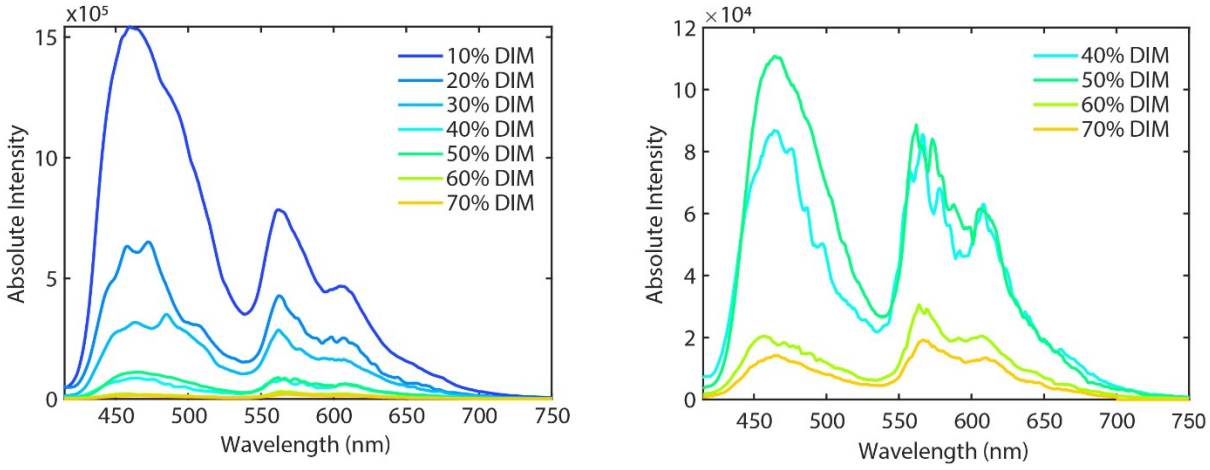

Figure S1. [Pt(thpy)(dppm)]ClO_4 emission spectra under 405 nm excitation with the broad fluorescence peak at 475 nm and overlapping phosphorescent peaks at 570 and 600 nm. As the DIM:DCM ratio of the solvent increases, the overall amount of emission decreases and the relative amount of phosphorescence to fluorescence increases.

X. [Pt(thpy)(dppm)]ClO_4 Lifetimes

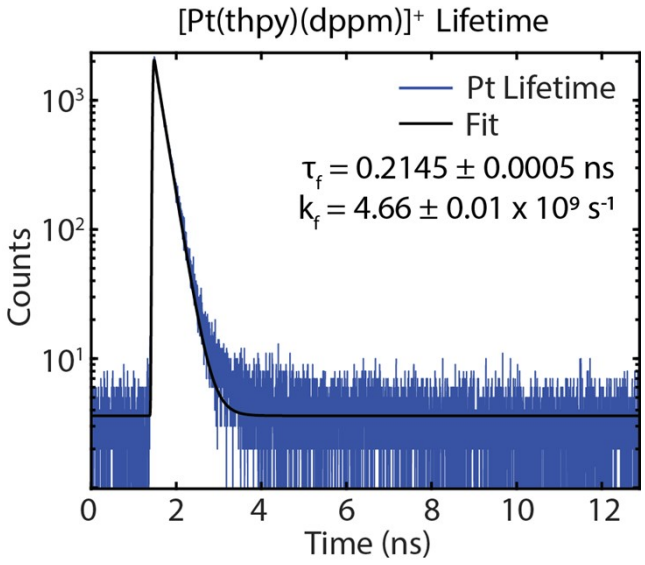

Figure S2. The photoluminescent lifetime of [Pt(thpy)(dppm)]ClO_4 in DCM was measured to be τ = 0.2145 ± 0.0005 ns.

The lifetime of [Pt(thpy)(dppm)]ClO_4 was measured at 80 MHz with a 405 nm pulsed laser. An exponential convoluted with a gaussian was used as a model function for the fit. The function is as follows:

$$A * \exp\left(-k(t-d)\right) * \exp\left(-\frac{\sigma^2 k}{2}\right)\left[1 + \operatorname{erf}\left(\frac{(t-d)-\sigma^2 k}{\sigma\sqrt{2}}\right)\right] + C \qquad \text{(S13)}$$

Where A is a pre-exponential factor, k is the rate, and σ is the width of gaussian. The fitting results are shown below with subsequent error.

Table S3. [Pt(thpy)(dppm)]$^+$ fluorescent lifetime fitting parameters.

A	$1.2 \pm 1.9 \times 10^3$
C	3.6 ± 0.2
d	1.4490 ± 0.0001
$k\ (s^{-1})$	$4.66 \pm 0.01 \times 10^9$
$\sigma\ (ns)$	0.0166 ± 0.0001

XI. [Pt(thpy)(dppm)]ClO_4 Quantum Yield Measurements

Absolute quantum yield measurements were conducted on a Horiba Scientific PTI QuantaMaster400 spectrometer equipped with a petite integrating sphere. The absolute quantum yield of [Pt(thpy)(dppm)]ClO4 was measured in DCM The complex [Pt(thpy)(dppm)]ClO^4 was diluted in DCM to have an optical density of 0.10 O.D.

XII. [Pt(thpy)(dppm)]ClO_4 FOC Fitting

The FOC of each [Pt(thpy)(dppm)]ClO_4 in DCM:DIM solution was fit using the results of the kinetic model. The resulting theoretical FOCs are overlaid with the experimental data in Figure 3c. The results of the fitting are found in table S3. For simplicity, reverse intersystem crossing was assumed to be negligent in the model and a constant fluorescence rate of $k_f = 1 \times 10^9$ s was assumed. The fitted rates are provided in the below table:

Table S4. Experimentally Obtained Fitted Rates and Quantum Yields of [Pt(thpy)(dppm)]ClO_4

%DIM in DCM	k_p(x10^6 s^{-1})	k_{ISC}(x10^6 s^{-1})	Φ_{fr}(x 10^{-3})	$\Phi_{eff\ pr}$ (x 10^{-3})
10	2.0±0.2	5.0±0.5	2.7±0.3	1.2±0.1
20	1.5±0.2	6.0±0.6	1.8±0.2	1.0±0.1
30	1.3±0.1	7.7±0.8	1.7±0.2	1.1±0.1
40	1.2±0.1	9.0±0.9	0.61±0.06	0.57±0.06
50	1.1±0.1	10±1	1.2±0.1	0.92±0.09
60	1.0±0.1	11±1	0.34±0.03	0.46±0.04
70	0.90±0.09	12.±1	0.34±0.03	0.43±0.04

Table 54. Calculated Rates and Quantum Yields of [Pt(thpy)(dppm)]ClO_4

%DIM in DCM	k_{fnr}(x10^9 s^{-1})	k_{pr}(x10^6 s^{-1})	k_{pnr}(x10^6 s^{-1})	Φ_{pr}
10	4.65±0.01	2.2±0.9	-0.2±0.9	0.44± 0.06
20	4.66±0.01	1.18± 0.8	0.3±0.8	0.58±0.08
30	4.66±0.01	0.88±0.8	0.4±0.8	0.65±0.09

40	4.66±0.01	0.36±0.8	0.8±0.8	0.9±0.1
50	4.66±0.01	0.48±0.8	0.6±0.8	0.8±0.1
60	4.66±0.02	0.19±0.8	0.8±0.8	1.3±0.2
70	4.66±0.02	0.15±0.8	0.8±0.8	1.3±0.2

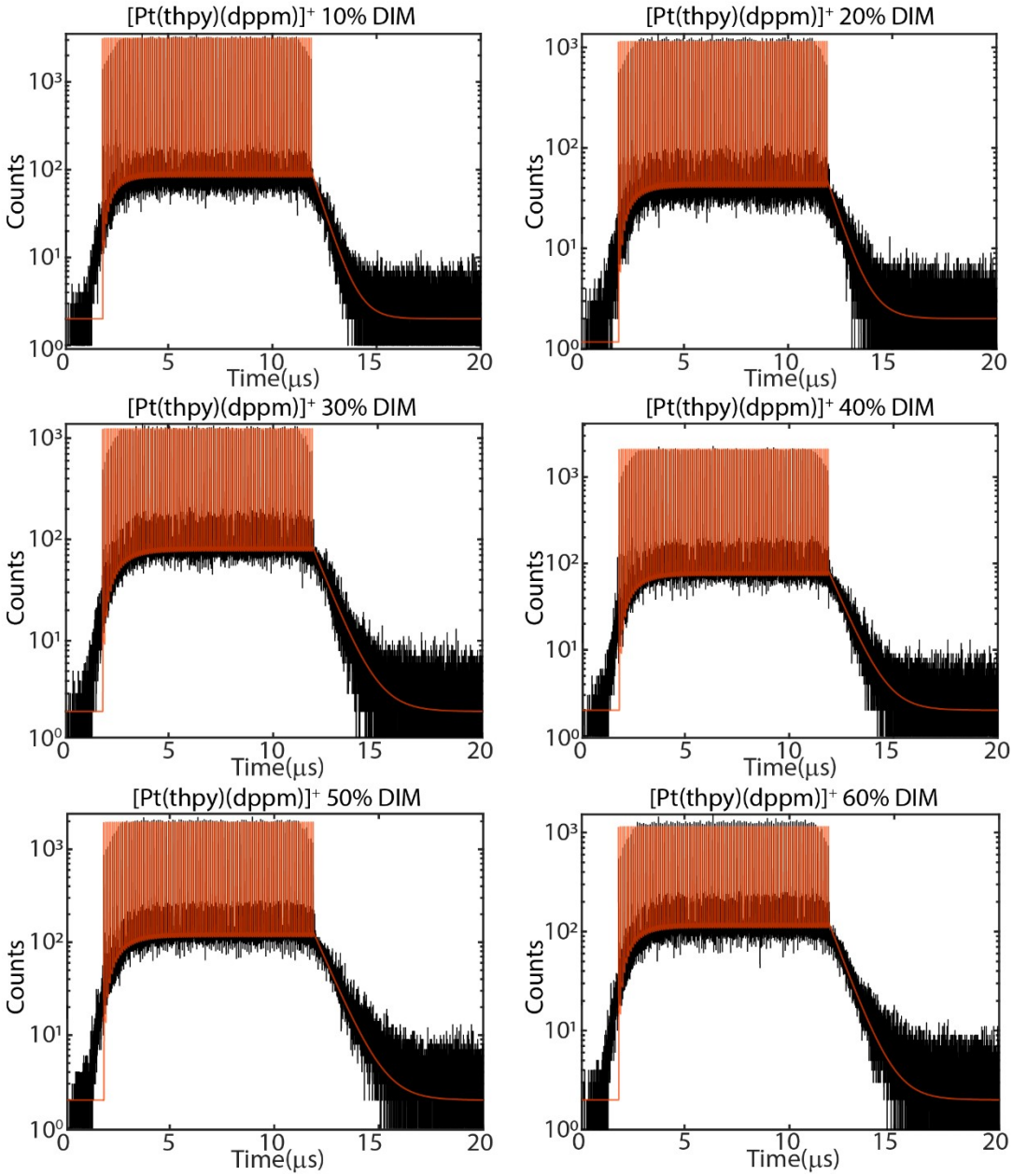

Figure S3. FOC traces of [Pt(thpy)(dppm)]ClO_4 in varying DIM concentrations (black) accompanied by fitting to the kinetic model (orange). Rate constants obtained from fitting are in Table S3.

XIII. Highly Phosphorescent Boron Clusters

As an additional proof of principle, several fluorescent boron clusters, 4,4′-Br_2-anti-$B_{18}H_{20}$ and 4,4′-I_2-anti-$B_{18}H_{20}$, were synthesized and studied based on the procedures established by *Anderson K. et al.*[4] Briefly, the sample was loaded at 2 wt% into a poly(methyl methacrylate) film (PMMA). The absorption and emission of the clusters shows a strong stokes shift that is attributed to the predominance of phosphorescent emission (Figure S4a).

The sample was then excited using a 405 nm laser and filtered with a 420 LP filter (Newport Optics, 5CGA-420). The 4,4′-I_2-anti-$B_{18}H_{20}$ was excited at an 1 MHz rep rate for 1, 2, 4, 8, and 16 pulses, or burst times of 1, 2, 4, 8, and 16 μs with a window time of 130 μs (Figure S4b). The 4,4′-Br_2-anti-$B_{18}H_{20}$ was excited at a 2.5 MHz rep rate for 1,10, 100, and 500 pulses, or burst times of 0.4, 4, 40, and 200 μs with an off time of 99.6, 696, 660, and 1200 μs (Figure S4c). In both the 4,4′-I_2-anti-$B_{18}H_{20}$ and 4,4′-Br_2-anti-$B_{18}H_{20}$, the longer the burst time, the higher the phosphorescent signal and therefore the larger the optically shelved triplet population. However, the 4,4′-I_2-anti-$B_{18}H_{20}$ reaches triplet state population equilibrium only after around 10 pulses whereas the 4,4′-Br_2-anti-$B_{18}H_{20}$ reaches triplet state population equilibrium after around 100's of pulses. This is attributed to a larger internal heavy atom effect from iodine compared to bromine in the anti-boron clusters.

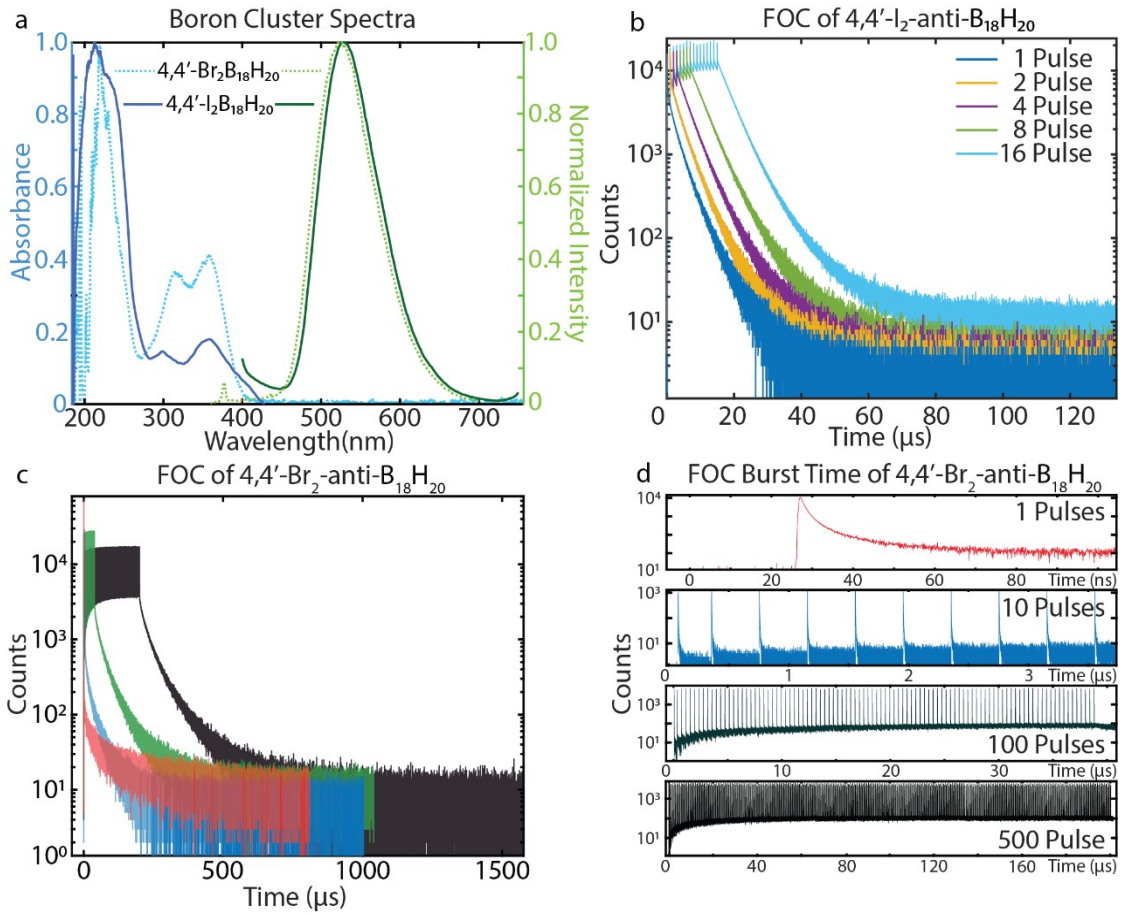

Figure S4. (a) UV-Vis absorption and emission spectra of 4,4′-Br_2-anti-$B_{18}H_{20}$ (abs: sky blue dotted line, emission: lime green dotted line) and 4,4′-I_2-anti-$B_{18}H_{20}$ (abs: dark blue solid line, emission: dark green dotted line). The phosphorescent emission demonstrates a strong stokes shift. (b) FOC of 4,4′-I_2-anti-$B_{18}H_{20}$ with various burst times/excitation pulses (1, 2, 4, 8, and 16 µs or pulses). (c) FOC of 4,4′-Br_2-anti-$B_{18}H_{20}$ with various burst times/excitation pulses (0.4, 4, 40, and 200 µs or 1, 10, 100, and 500 pulses). In both (b) and (c), and increase in the burst time leads to a higher optically shelved triplet state population. However, the 4,4′-I_2-anti-$B_{18}H_{20}$ in (b) reaches the triplet population equilibrium with less pulses than 4,4′-Br_2-anti-$B_{18}H_{20}$ in (c) due to the increased internal heavy atom effect of iodine over bromine. (d) The burst times of the 4,4′-Br_2-anti-$B_{18}H_{20}$ FOC traces show low pulse train to pulse train jitter and are recorded in high 64 ps resolution.

XIV. Flowed Sample Experiment Setup

A solution of Rose Bengal in water was bubbled with oxygen gas to saturate the solution with oxygen. The Rose Bengal in water solution was placed in a cell chamber (Aireka Cells, SC15032-Coverslip Cell Chamber) and a peristaltic pump (Pharmacia BioTech, Pump P-1) was used to flow sample through the cell chamber. Flowing the sample repleted the emitters lost to photobleaching as a result of multiple pulsed excitation.

Referenced

1. Lai, S. W., Chan, M. C. W., Cheung, T. C., Peng, S. M. & Che, C. M. Probing d8-d8 interactions in luminescent mono- and binuclear cyclometalated platinum(II) complexes of 6-phenyl-2,2'-bipyridines. *Inorg Chem* **38**, 4046–4055 (1999).

2. Lai, S. W., Chan, M. C. W., Cheung, K. K., Peng, S. M. & Che, C. M. Synthesis of organoplatinum oligomers by employing N-donor bridges with predesigned geometry: Structural and photophysical properties of luminescent cyclometalated platinum(II) macrocycles. *Organometallics* **18**, 3991–3997 (1999).

3. Li, K. *et al.* Excitation-Wavelength-Dependent and Auxiliary-Ligand-Tuned Intersystem-Crossing Efficiency in Cyclometalated Platinum(II) Complexes: Spectroscopic and Theoretical Studies. *Inorg Chem* **59**, 14654–14665 (2020).

4. Anderson, K. P. *et al.* Benchmarking the dynamic luminescence properties and UV stability of B18H22-based materials. *Dalton Transactions* **51**, 9223–9228 (2022).